AGU PUBLICATIONS

JGR

Journal of Geophysical Research: Solid Earth

RESEARCH ARTICLE
10.1002/2016JB013432

**Key Points:**
- We estimate the spatial distribution of afterslip from ~6.3 year long postseismic time series recorded by the SuGAr network, with PCAIM
- We account for viscoelastic deformation in our models by jointly inverting for on-fault afterslip and off-fault strains
- The shallow afterslip in our models loaded the 2010 Mentawai earthquake rupture zone and potentially promoted its rupture

**Supporting Information:**
- Supporting Information S1

**Correspondence to:**
L. L. H. Tsang,
lhtsang1@e.ntu.edu.sg

**Citation:**
Tsang, L. L. H., E. M. Hill, S. Barbot, Q. Qiu, L. Feng, I. Hermawan, P. Banerjee, and D. H. Natawidjaja (2016), Afterslip following the 2007 $M_w$ 8.4 Bengkulu earthquake in Sumatra loaded the 2010 $M_w$ 7.8 Mentawai tsunami earthquake rupture zone, *J. Geophys. Res. Solid Earth*, *121*, 9034–9049, doi:10.1002/2016JB013432.

Received 1 AUG 2016
Accepted 21 NOV 2016
Accepted article online 24 NOV 2016
Published online 21 DEC 2016



# Afterslip following the 2007 $M_w$ 8.4 Bengkulu earthquake in Sumatra loaded the 2010 $M_w$ 7.8 Mentawai tsunami earthquake rupture zone

**Louisa L. H. Tsang[1,2], Emma M. Hill[1,2], Sylvain Barbot[1,2], Qiang Qiu[1,2], Lujia Feng[1], Iwan Hermawan[1,3], Paramesh Banerjee[1], and Danny H. Natawidjaja[3]**

[1]Earth Observatory of Singapore, Nanyang Technological University, Singapore, [2]Asian School of the Environment, Nanyang Technological University, Singapore, [3]Research Center for Geotechnology, Indonesian Institute of Sciences, Bandung, Indonesia

**Abstract** The 12 September 2007 $M_w$ 8.4 Bengkulu earthquake in Sumatra marked the first in a modern series of large earthquakes along the Mentawai section of the Sunda megathrust. Understanding the spatial distribution of coseismic slip and ensuing afterslip is important for assessing seismic hazard in neighboring unruptured regions of the megathrust. We reestimate the spatial distribution of coseismic slip during this earthquake with improved coseismic offsets from the Sumatran GPS Array (SuGAr) and estimate afterslip following this earthquake with SuGAr postseismic time series spanning ~6.3 years after the earthquake. We invert for the spatiotemporal distribution of afterslip with the principal component analysis-based inversion method (PCAIM), and we take into account viscoelastic deformation by incorporating into the inversion the estimation of strain within ductile deforming blocks located at asthenospheric depths. Our results suggest cumulative afterslip concentrated within, updip, and downdip of the 2007 coseismic rupture area and shallow afterslip that borders and overlaps the 2010 $M_w$ 7.8 Mentawai earthquake rupture zone. The cumulative contribution of stress changes due to the coseismic event and the ensuing afterslip likely increased strain rates in the shallow portion of the megathrust adjacent to the Mentawai earthquake rupture area, potentially promoting its rupture in 2010.

## 1. Introduction

On the 12 September 2007, a $M_w$ 8.4 earthquake occurred along the southern part of the Mentawai section of the Sunda megathrust—a section that has been forecast to rupture in the coming decades [*Sieh et al.*, 2008]. The Mentawai section last ruptured in 1797 and 1833, producing earthquakes of $M_w$ 8.6–8.8 and $M_w$ 8.8–8.9, respectively [*Philibosian et al.*, 2014; *Sieh*, 2007]. The moment released by the 2007 Bengkulu event represents only a fraction of that released along the same section of the megathrust in 1797 and 1833, as well as of the moment deficit accumulated since 1833, suggesting that the potential for a great earthquake along this section remains high [*Konca et al.*, 2008].

In the months and years following the 2007 Bengkulu earthquake, Sumatran GPS Array (SuGAr) stations located close to the coseismic rupture area recorded substantial amounts of postseismic deformation. This observation leads to an important question: How much of the remaining moment deficit since 1833 has been released by afterslip?

In addition, during ongoing postseismic deformation following the 2007 event, an unusual earthquake occurred ~3.1 years after the Bengkulu earthquake—on 25 October 2010, a $M_w$ 7.8 tsunami earthquake [*Hill et al.*, 2012; *Yue et al.*, 2014] nucleated in the shallow region updip of the Bengkulu earthquake rupture zone (Figure 1). The spatial proximity between these two earthquakes begs further questions: How does afterslip redistribute stress on this part of the megathrust? Did afterslip promote the 2010 rupture? Answering these questions is relevant for elucidating the physical conditions and processes that promote nucleation of tsunami earthquakes in the shallow region of the megathrust; a region that was commonly hypothesized to be incapable of hosting large earthquakes [e.g., *Byrne et al.*, 1988].

To address these questions, we study postseismic time series that span multiple years following the earthquake. Even though a previous study examined the afterslip following the Bengkulu earthquake, the

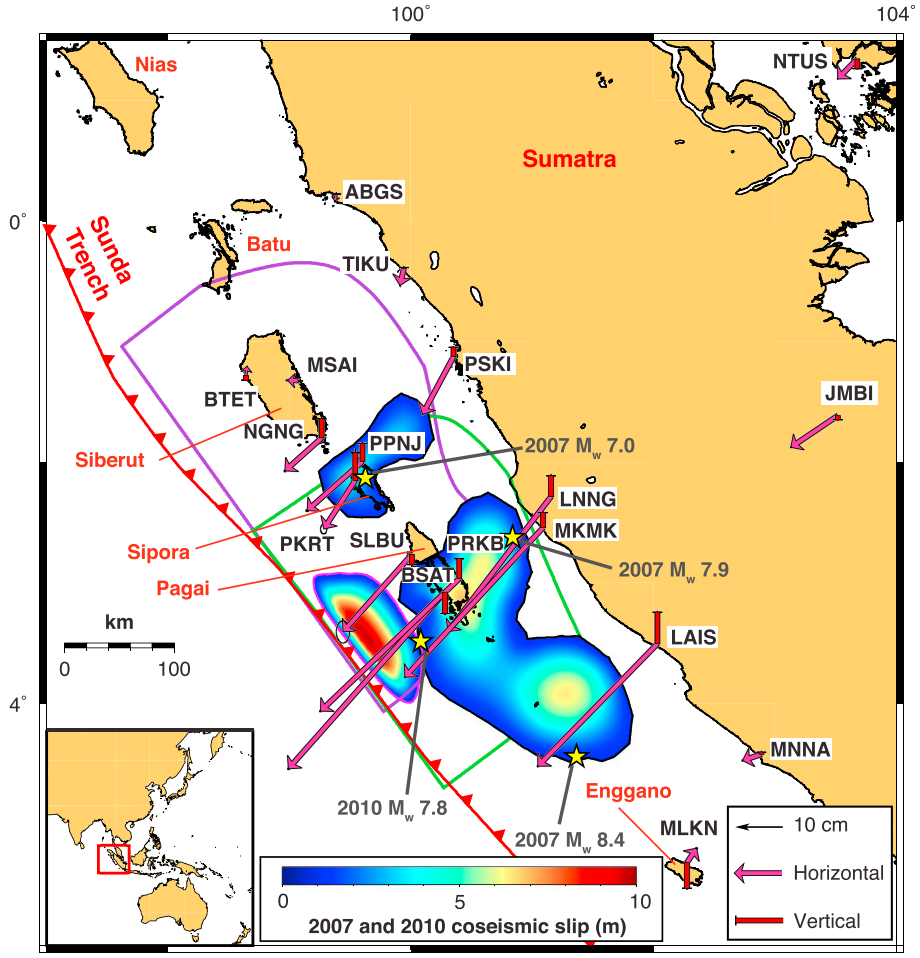


**Figure 1.** Map of the 17 Sumatran GPS Array (SuGAr) stations and 1 IGS station (NTUS) used to invert for coseismic slip and afterslip, and cumulative ~6.3 year postseismic horizontal (arrows) and vertical (bars) displacements. Colored slip represents the 2007 Bengkulu earthquake main shock and aftershock source models from our study (1 m coseismic slip contour outlined in black), and the 2010 Mentawai tsunami earthquake source model from *Hill et al.* [2012] (1 m slip contour outlined in magenta). Stars: Hypocenters of each earthquake, from the ANSS catalog. Purple and green lines outline the rupture areas of the 1797 and 1833 earthquakes, respectively, as determined by *Philibosian et al.* [2014].

maximum time period of their data spans only 15 months after the earthquake [*Lubis et al.*, 2012]. To the best of our knowledge, postseismic deformation spanning longer time periods after the earthquake have not yet been studied. In our study, we model the long post-Bengkulu earthquake time series of displacements recorded by SuGAr stations—a time period that spans an ~6.3 year long period until the end of 2013 and which includes the period up to and beyond the 2010 Mentawai earthquake.

Our study is novel in the following aspects:

1. we reestimate the coseismic slip distribution of the 2007 Bengkulu earthquake with improved coseismic SuGAr offsets estimated by *Feng et al.* [2015] and a more realistic fault geometry compared to previous studies; and
2. we account for viscoelastic deformation in our models by jointly inverting for afterslip on the fault and strain within finite volume blocks located at asthenospheric depths, which accommodate ductile deformation due to viscous flow.

As both coseismic slip and afterslip are estimated on a consistent fault geometry, the results of our study enable us to easily compare between regions of the fault that slipped coseismically and postseismically, and gain a comprehensive picture of the spatiotemporal distribution of coseismic stresses relaxed as afterslip. The results of our study contribute insights into the importance of coseismic and afterslip history in promoting coseismic failure of the shallowest portions of megathrusts.

## 2. GPS Data

We use GPS data from 17 SuGAr stations and 1 IGS station (NTUS) which were operating at the time of the 2007 Bengkulu earthquake and which recorded afterslip following the event (Figure 1). We processed the GPS data using the GPS-Inferred Positioning System and Orbit Analysis Simulation Software (GIPSY-OASIS) version 6.2 [*Zumberge et al.*, 1997]. Full details of the data processing are described in *Feng et al.* [2015]. We transformed the daily positions in the ITRF2008 (International Terrestrial Reference Frame 2008) into daily positions relative to the Sunda plate, using the ITRF2008-Sunda transformation [*Altamimi et al.*, 2012].

*Feng et al.* [2015] estimated GPS coseismic offsets and postseismic decays, together with long-term rates, and annual and semiannual seasonal signals, on all three components of each station using a nonlinear least squares optimization procedure. The resulting coseismic offsets estimated from the optimization procedure represent more accurate and more spatially coherent estimates compared to previous studies. Using their estimates, we were able to model the postseismic GPS time series for the 2007 event with the following signals removed: long-term rates, seasonal signals, coseismic offsets, and postseismic decays associated with other earthquakes that occurred during the 2007 postseismic period (more details in Text S1 in the supporting information).

Our GPS postseismic time series span ~6.3 years, starting from the day of the earthquake (12 September 2007) until the end of 2013 (31 December 2013). We note that two aftershocks of $M_w$ 7.9 and 7.0 occurred ~12 and ~16 h after the main shock, respectively (Figure 1); the coseismic offsets associated with these events were estimated together with the $M_w$ 8.4 main shock.

In Table S1, we list the GPS coseismic displacements and the cumulative GPS postseismic displacements over the ~6.3 year long postearthquake time period. The cumulative postseismic displacements range from ~+15 to −70 mm on the east component, ~+5 to −100 mm on the north component, and ~−60 to −15 mm on the vertical component. The largest cumulative horizontal postseismic displacements were observed at stations BSAT and PRKB, adjacent to the parts of the fault that experienced peak coseismic slip during the $M_w$ 8.4 main shock (Figure 1). These two stations also recorded the largest GPS coseismic displacements.

For our coseismic slip models, we additionally included 18 coral uplift measurements reported by *Konca et al.* [2008] (Table S2). These measurements provide improved model resolution under the Pagai Islands and Sipora (Figure S5) and therefore better bounds on coseismic slip in these regions. These measurements were taken up to a month after the earthquake, so they include a portion of postseismic deformation. We note that the GPS offsets and coral data record both the $M_w$ 8.4 main shock and the $M_w$ 7.9 and 7.0 aftershocks, so our inverted slip distributions (described in the next section) represent coseismic slip from all three events.

## 3. Inversion Methods

We inverted for coseismic slip and afterslip on a model fault that spans the length of the Mentawai section from the Batu Islands in the northwest to Enggano Island in the southeast. The dip profile of the fault approximates the Slab 1.0 model [*Hayes et al.*, 2012] along this section of the megathrust (Figure 2a) and extends to 100 km depth. We discretized the fault into 20 km by 20 km rectangular subfault patches and inverted for slip on each patch using a linear least squares inversion technique, with positivity constraints. Displacements at each GPS station were calculated with Okada's solutions for deformation due to dislocations embedded in an elastic half-space [*Okada*, 1985] and with semianalytic solutions for the surface displacements due to distributed shear in finite volumes. We used a modified version of the reduced chi-square, $\chi_r^2$, to evaluate quantitatively the fit of the data and the model displacements (Text S1). Further details of Laplacian smoothing and additional constraints implemented in the inversion are described in Text S1.

### 3.1. Estimating Afterslip With the Principal Component Analysis-Based Inversion Method (PCAIM)

We inverted for the spatial and temporal distribution of afterslip with the principal component analysis-based inversion method (PCAIM) [*Kositsky and Avouac*, 2010]. The advantages of the PCAIM method are that it is able to deal with time periods with missing data, and it effectively filters data time series for the main postseismic signal by representing the time series with an optimum number of principal components. To select the optimum number of principal components, we examined the cumulative amount of variance in the data explained by incrementally adding principal components to represent the time series. Representing the time series with one principal component explains ~74% of the variance in the data, while adding a second

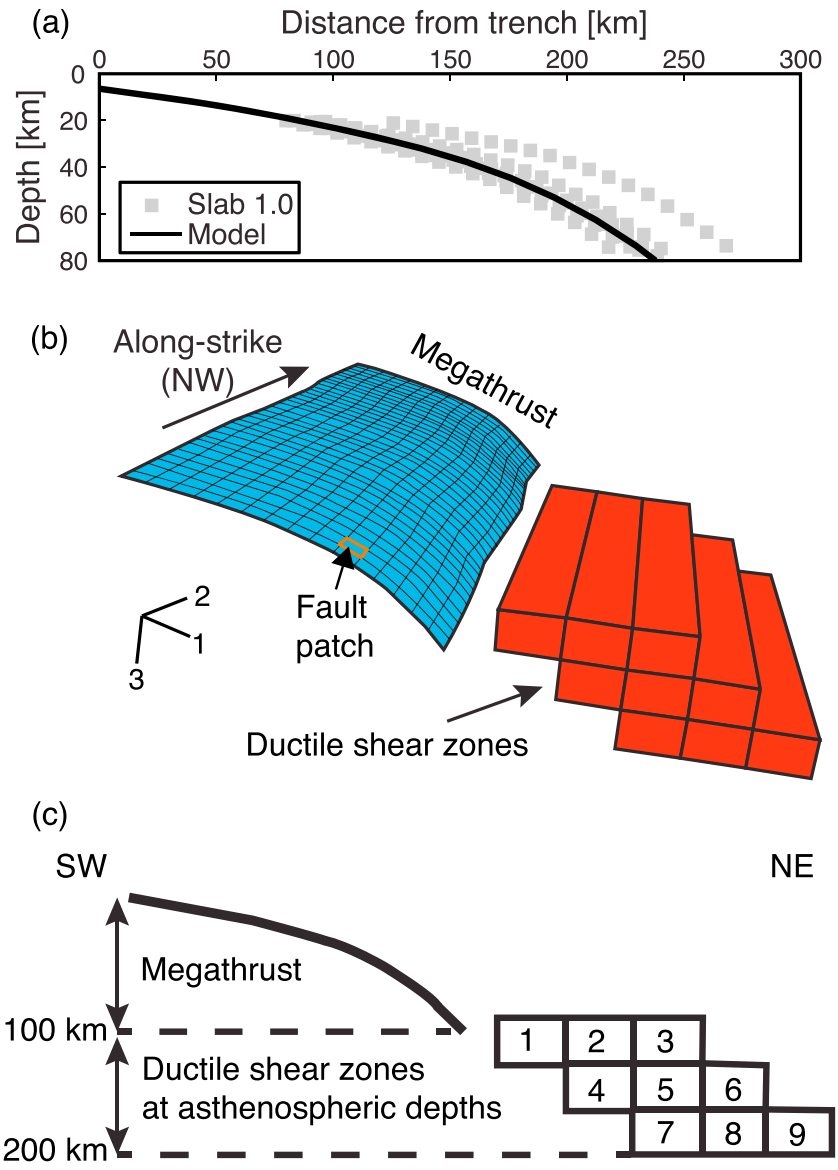


**Figure 2.** (a) Dip profile of our fault model approximates the Slab 1.0 model [*Hayes et al.*, 2012] along this section of the megathrust. Grey squares define the fault geometry of Slab 1.0 from a suite of depth cross sections along this section of the megathrust. (b) Oblique view and (c) cross-sectional view showing relative location and geometry of the fault model at <100 km depths, and nine ductile shear zones (numbered) located at ~100–200 km asthenospheric depths.

principal component explains ~94% of the data variance (Figure S1). Adding further principal components explains only marginally more of the cumulative amount of variance in the data. Theoretically, the higher-order principal components represent other signals in the time series, such as seasonal signals, but we should be wary of directly interpreting the spatial patterns suggested by each principal component as being from a particular tectonic or physical process. We chose to represent the time series with one principal component, as addition of one or more components does not change the afterslip model significantly (Figure S2).

### 3.2. Joint Inversion of Afterslip and Viscoelastic Deformation With PCAIM

Due to release of fluids into the mantle wedge from the subducting oceanic lithosphere, the viscosity of the mantle prism is 1 to 2 orders of magnitude lower than the oceanic lithosphere [*Karato*, 2010]. Viscous flow in the mantle prism occurs due to coseismic stress changes imparted by the main shock and aftershock ruptures and their afterslip. The timescale of the resulting viscoelastic deformation depends on the viscosity of the mantle prism. Previous researchers investigating postseismic deformation following the Sumatran

earthquakes estimated mantle viscosities in this region between $10^{17}$ to $10^{19}$ Pa s [*Lubis et al.*, 2012; *Panet et al.*, 2007; *Pollitz and Banerjee*, 2006]. The value of the mantle viscosity can depend on the time window of geodetic observations examined; examining geodetic observations late in the interseismic period of the earthquake cycle can yield mantle viscosities on average 1 order of magnitude higher than geodetic observations early in the interseismic period of the earthquake cycle [*Meade et al.*, 2013]. In addition, some studies of early stage postseismic deformation assume predominantly viscoelastic deformation and do not account for afterslip, employing instead transient rheologies to explain different time-dependent decay patterns of geodetic time series [e.g., *Panet et al.*, 2007]. As we are modeling a multi year long time series of postseismic displacements, it is important to account for the relative contribution of both afterslip and viscoelastic deformation to the postseismic time series. Further, *Feng et al.* [2015] found that a wide range of logarithmic decay times are needed to fit the postseismic time series, which they propose represents the cumulative effects of several different postseismic relaxation mechanisms. Additionally, many studies model the postseismic deformation as due to pure afterslip [e.g., *Hsu et al.*, 2006] thereby biasing the spatial distribution of afterslip [*Bruhat et al.*, 2011].

Traditionally, geodetic studies first remove the contribution of viscoelastic deformation from postseismic time series by forward modeling viscoelastic deformation based on reasonable assumptions of the coseismic slip distribution and the Earth model [e.g., *Suito and Freymueller*, 2009], then inverting the residual postseismic time series for afterslip distributions. This method assumes that viscoelastic deformation is driven only by coseismic stress changes, but neglects the contribution of viscoelastic deformation driven by time-dependent afterslip, which may be a significant contribution if afterslip occurs at predominantly deeper depths on the megathrust. Also, this method suffers from our insufficient knowledge of the Earth model and inaccuracies in the coseismic slip distribution. Other studies model the coupling between afterslip and viscoelastic flow in stress-driven models of postseismic relaxation [*Barbot and Fialko*, 2010a; *Rousset et al.*, 2012; *Rollins et al.*, 2015], but the approach is computationally expensive. It also makes use of simplified physical models of deformation that are not amenable to kinematic inversions.

We therefore investigated an alternative method of determining the relative contributions of afterslip and viscoelastic deformation to the postseismic time series. We discretized the mantle volume into nine blocks of finite volume that can accommodate ductile deformation below the downdip end of the model fault, at asthenospheric depths (Figures 2b and 2c). We refer to these blocks as ductile shear zones. We expect that viscous flow occurs predominantly in the asthenosphere, and as the lithosphere-asthenosphere boundary is located at ~100 km depths at Sumatra [*Kumar et al.*, 2007], we placed the ductile shear zones at ~100–200 km depths (Figures 2b and 2c). The lengths of these zones extend the Bengkulu segment and are approximately aligned with the subducting slab at these depths.

We define a reference system $e_1$, $e_2$, and $e_3$, where $e_1$ and $e_2$ are the trench-perpendicular and trench-parallel directions, respectively, and $e_3$ the depth direction (Figure 2b). We then linearly inverted for each of the six independent strain components within each ductile shear zone. The addition of nine ductile shear zones with six components adds 54 unknown strain parameters into our inversion. The inversion recovers afterslip and strain, which have different units. We used units of centimeters and microstrain to build the afterslip and strain kernels, respectively (Text S2). We calculated Green's functions relating distributed inelastic strain in finite volumes to surface displacements with Relax 1.0.7 [*Barbot and Fialko*, 2010a, 2010b; *Barbot et al.*, 2009]. We then loaded the Green's functions into PCAIM, enabling joint inversion of afterslip on the fault and strain components in ductile shear zones. As viscous flow is deviatoric, this implies that $\epsilon_{11} + \epsilon_{22} + \epsilon_{33} = 0$. We added this deviatoric strain constraint to the design matrix, as well as constraints on the strain directions based on predicted coseismic traction directions in each shear zone (Text S2). In addition, we experimented with a range of Laplacian smoothing weights for afterslip and strain, and selected the combination of weights that yields spatially consistent afterslip and strain distributions. We note that model resolution is limited in the deeper shear zones (Figures S3 and S4), so we additionally present a suite of models to illustrate the sensitivity of the model to various smoothing parameters.

## 4. Results

### 4.1. Coseismic Slip Distribution

Figure 3 shows the results of our inverted coseismic slip distribution for the $M_w$ 8.4, 7.9, and 7.0 earthquakes, based on GPS and coral data (Figure S5 shows the results of inverting only GPS data). Our model yields $\chi_r^2 = 1.2$ and a geodetic moment of $4.18 \times 10^{21}$ N m. The spatial pattern of our coseismic model is very similar to that

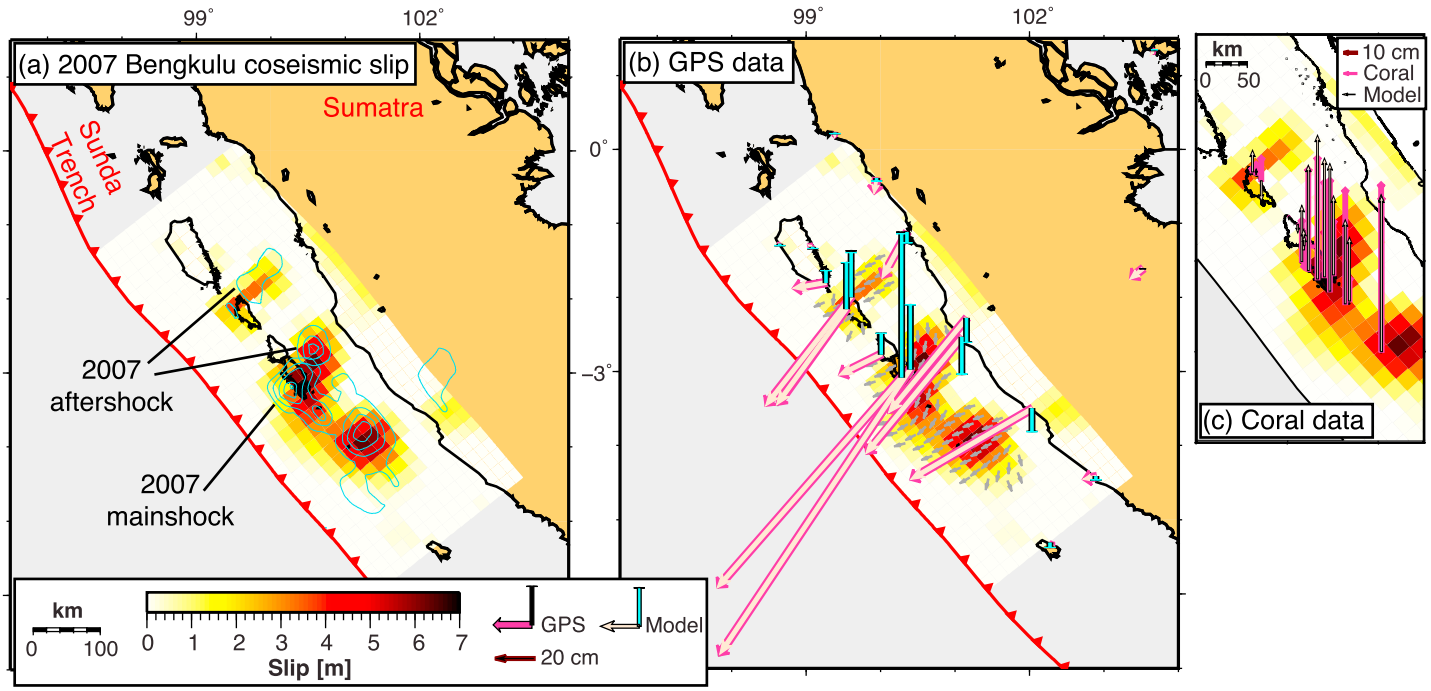


**Figure 3.** (a) Coseismic slip distribution of the 2007 Bengkulu earthquake $M_w$ 8.4 main shock and $M_w$ 7.9 and 7.0 aftershocks. Our model is similar to the coseismic model of *Konca et al.* [2008] (1, 3, 5, and 7 m slip contours shown in cyan), although the locus of peak coseismic slip under the Pagai Islands is located farther downdip. The maximum coseismic slip in our model is ~7 m. (b) Data and model GPS displacements at 17 SuGAr stations and one IGS station, and (c) data and model vertical displacements at the 18 coral sites.

of *Konca et al.* [2008], although the locus of peak coseismic slip is located farther downdip (Figure 3a). This may be related to our use of a more realistic curved fault geometry, rather than a planar fault with a constant dip. The maximum coseismic slip in our model is ~7 m, comparable to the maximum slip value in *Konca et al.*'s [2008] model. We note that although the value of peak slip is poorly resolved and depends on the choice of Laplacian smoothing, varying the smoothing weight over 3 orders of magnitude results in a small difference in estimated geodetic moments (Table S3). The geodetic moment is therefore robustly estimated. In addition, the locus of peak coseismic slip does not vary with the Laplacian smoothing weight.

### 4.2. Model 1: Afterslip Models That Do Not Account for Viscoelastic Effects

Figure 4 shows our model of cumulative afterslip over an ~6.3 year period following the Bengkulu earthquake, and Figure S6 shows the time series of data model fits. Figure S7 shows the spatio temporal evolution of afterslip. Our model yields $\chi_r^2 = 18.5$ and a geodetic moment of $3.55 \times 10^{21}$ N m, equivalent to a moment magnitude of $M_w$ 8.3. The cumulative afterslip moment amounts to ~85% of the coseismic geodetic moment. Our results suggest peak afterslip concentrated in two regions located updip and downdip of the 2007 coseismic rupture area: ~2.5 m of peak cumulative afterslip is located immediately downdip of the 2007 coseismic rupture area (region A, Figure 4a), at ~30–75 km depths on the megathrust; and ~2 m of cumulative afterslip is concentrated updip of the 2007 main shock rupture area at <12 km depths on the megathrust, which borders and overlaps the Mentawai earthquake rupture area (region B). In addition, a moderate amount of cumulative afterslip (~1–2 m) occurred within the 2007 main shock rupture area (region D) and close to the 2007 $M_w$ 7.9 aftershock area (region C). Strikingly, our model shows no afterslip under the Pagai Islands, which might indicate that coseismic slip in this location relieved the majority of the interseismic slip deficit. Alternatively, this location may represent a patch on the fault with purely velocity weakening behavior. We note that horizontal data model fits are poorest at ABGS, PSKI, MLKN, and NTUS, and the vertical data model fits are poorest at NTUS and MKMK (Figures 4b, S6, and S9); this may be because these components record viscoelastic deformation.

### 4.3. Model 2: Afterslip Models That Account for Viscoelastic Effects

Figure 5 shows our joint inversion results for afterslip on the megathrust and strain in ductile shear zones. Figure S8 shows the time series of data model fits and Figure S10 the spatiotemporal evolution of afterslip.

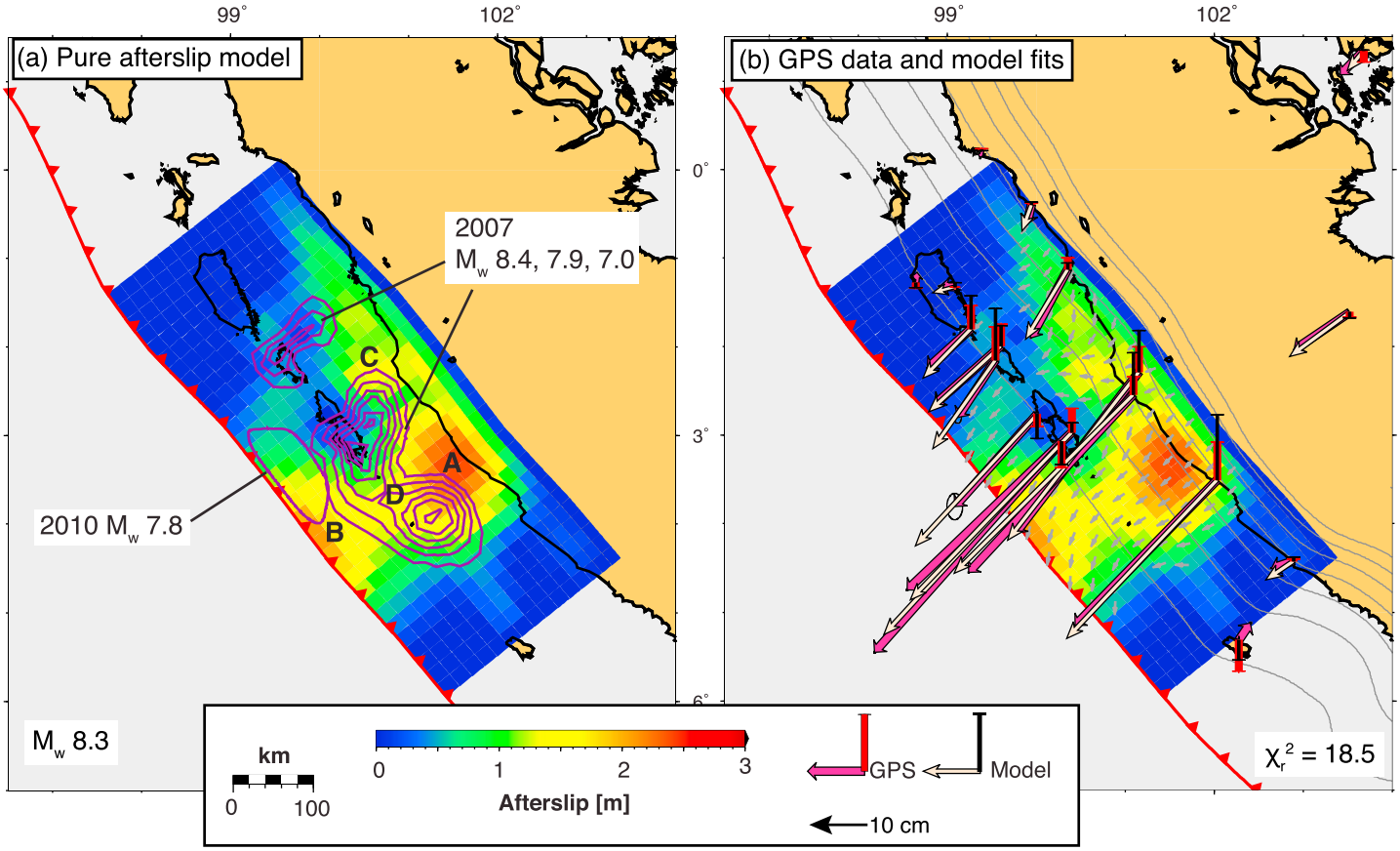


**Figure 4.** (a) Spatial distribution of cumulative afterslip in an ~6.3 year period following the 2007 earthquake, for models that do not account for viscoelastic effects, and relationship between the afterslip and the 2007 and 2010 earthquake rupture areas. Purple: 1 m slip interval contours of the 2007 Bengkulu main shock and aftershock sequence from our model in Figure 3; and 1 m slip contour of the 2010 earthquake [from *Hill et al.*, 2012]. Regions A to D are discussed in the text. (b) Comparison of data and model displacements. Grey contours: 20 km depth interval slab contours from the Slab 1.0 model.

This model suggests a geodetic moment of $4.03 \times 10^{21}$ N m, equivalent to a moment magnitude of $M_w$ 8.4. The cumulative afterslip moment amounts to ~95% of the coseismic geodetic moment. This model yields better data model fits (a lower modified reduced chi-square value, $\chi_r^2$, of 16.1) compared to model 1 which does not account for viscoelastic effects. An *F* test reveals that the improvement in fit is significant at the 95% confidence level (Text S2). This model yields improved data model fits on the horizontal components most notably at stations MNNA and NTUS, and vertical components at far-field stations JMBI and NTUS (Figure S9) —stations which likely reflect a greater proportion of viscoelastic deformation following the earthquake.

Figure 6 shows the difference in afterslip between model 2, that accounts for viscoelastic effects, and model 1, that does not account for viscoelastic effects. Strikingly, model 2 indicates a lesser amount of cumulative afterslip (~2.1 m) downdip of the 2007 coseismic rupture areas, ~0.4 m less than that in model 1 (regions A and C, Figures 5a and 6). Therefore, the estimated afterslip in the downdip region of model 1 likely represents a portion of viscoelastic deformation mapped onto the megathrust. In contrast, and similar to model 1, no afterslip occurred under the Pagai Islands. In the shallow region of the fault, a moderate amount of cumulative afterslip (~1.9 m) borders and overlaps the Mentawai earthquake rupture area (region B, Figure 5a); model 2 shows ~0.1 m less afterslip compared to model 1, although there is an ~0.3–0.4 m increase in afterslip bordering the northwestern edge of the Mentawai earthquake rupture zone (region F, Figure 6), and southwest of the 2007 coseismic rupture area (region E, Figure 6).

Figure 5b shows the spatial distribution of deviatoric strain in each shear zone (and Figures S12 and S13 show the time evolution of strain and strain directions within each shear zone, respectively). Due to limited model resolution in the shear zones (as shown in Figure S3), we cannot robustly constrain the spatial pattern of strain

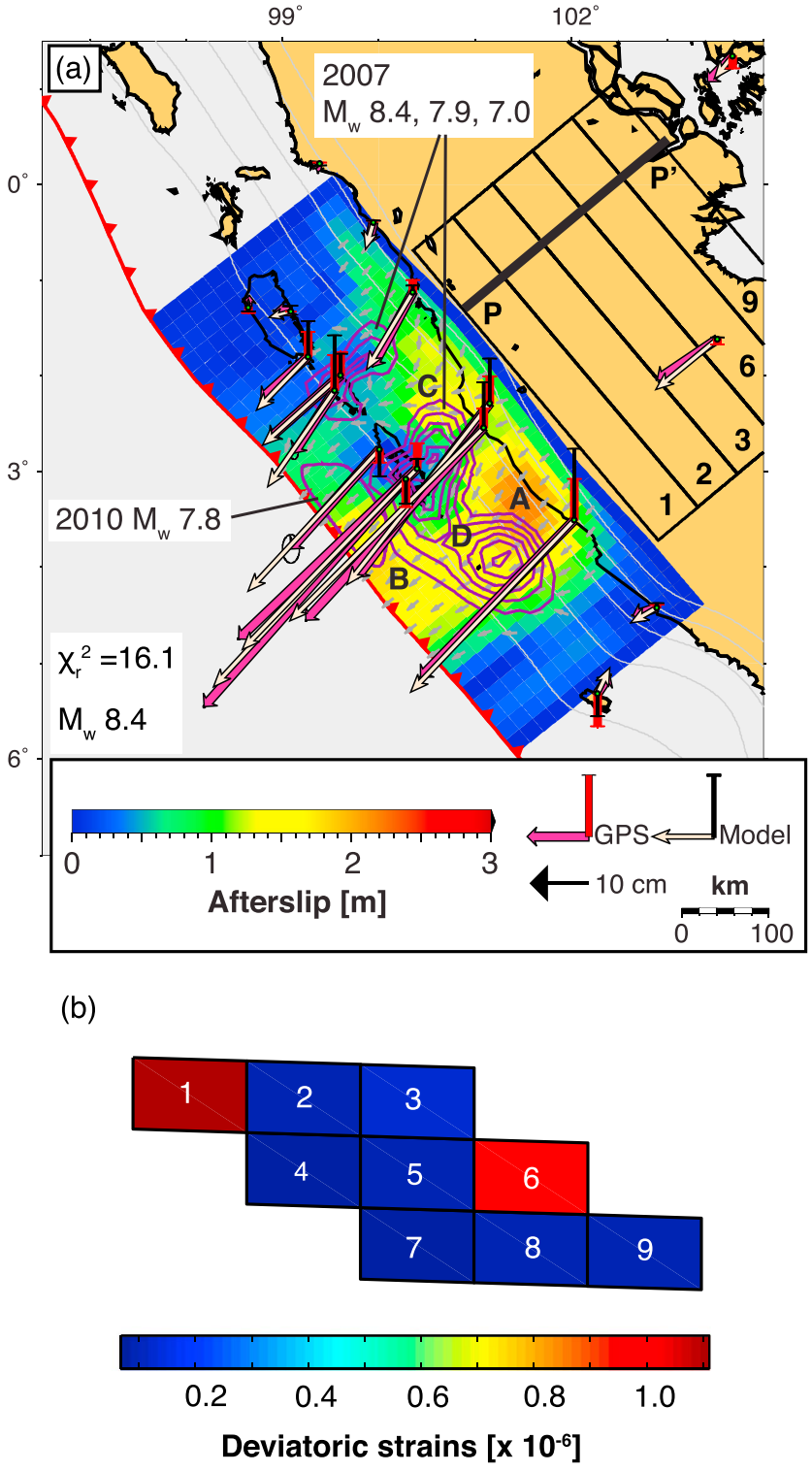


**Figure 5.** (a) Cumulative afterslip for model that accounts for viscoelastic effects, with GPS data and model displacements shown. The surface projections of the ductile shear zones are outlined in black (located under Sumatra); the number of the shear zone is labeled at its southeastern edge. Cross-section P to P′ is shown in Figure 5b. Grey contours: 20 km depth interval slab contours from the Slab 1.0 model. (b) Deviatoric strain within ductile shear zones. Cross-sectional ends of the shear zones are shown, with the top row being the shallowest row of blocks. Compared to the model shown in Figure 4, the magnitude of afterslip in region A in this model is less.

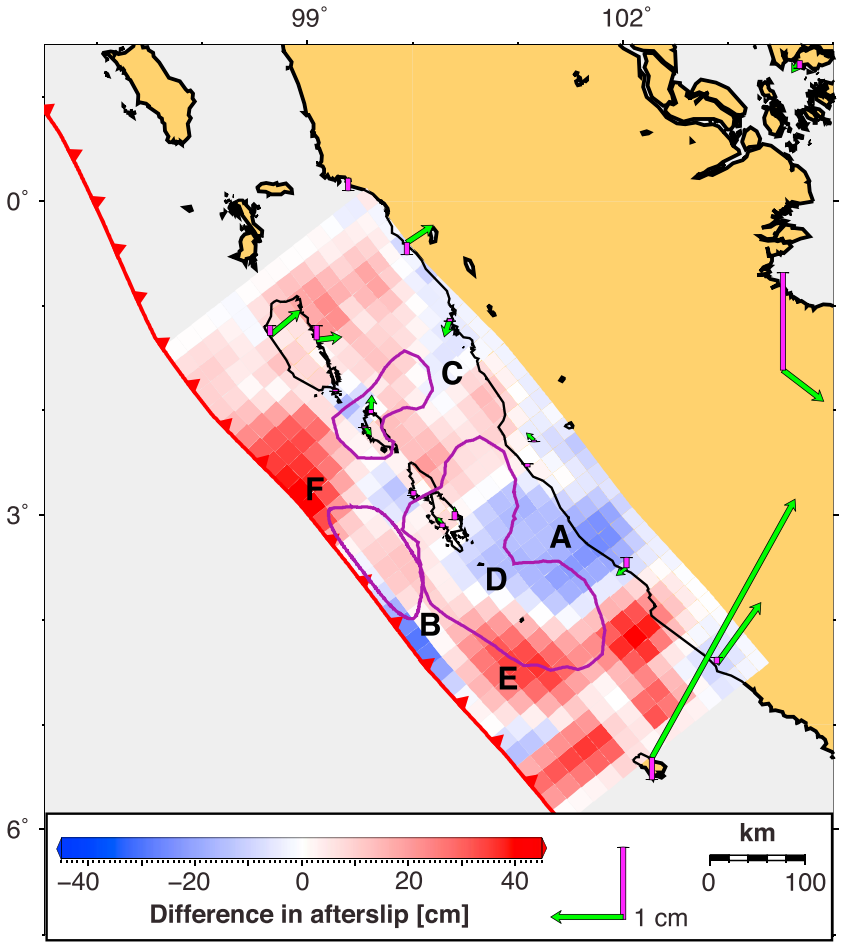


**Figure 6.** Difference in afterslip and model displacements between the two afterslip models, where model 1 (which does not account for viscoelastic effects) is subtracted from model 2 (which accounts for viscoelastic effects). In model 2, a lesser amount of afterslip is located in regions downdip of the 2007 coseismic rupture areas (regions A and C), while a greater amount of afterslip is located in the region bordering the southern, updip extent of the 2007 coseismic rupture area (region E), and northwest of the Mentawai earthquake rupture area (region F). Purple contours are the 1 m slip contours of the 2007 and 2010 coseismic ruptures.

in each shear zone. The strain in shear zone 6 is likely illluminated because station JMBI is located directly above this shear zone. Figure S14 shows a suite of models illustrating how afterslip and strain distributions vary with different smoothing parameters—although the spatial pattern of strain varies with different smoothing weights, the spatial distribution of afterslip is robust.

## 5. Model Resolution

We conducted checkerboard tests of different sized checks to assess the resolution of slip across our fault model. Figures 7a–7c show the input checkerboard of slip across our fault model with 60, 80, and 120 km sized square checks, respectively. The synthetic GPS displacements from the checkerboard tests were inverted for slip on the fault employing the same Laplacian smoothing weight as that employed in the afterslip models that do not account for viscoelastic effects.

Figures 7d–7f show the recovery of slip checks. The 120 km sized slip checks are well recovered under the Pagai Islands and in the NW region of the fault (under Sipora and Siberut), with the exception of regions closest to the trench (Figure 7f). The estimated slip checks are smoothed across neighboring fault patches in the region SE of the Pagai Islands.

For the 60 and 80 km sized checks, slip is reasonably well recovered under the islands, and slip is smoothed across neighboring fault patches. Slip checks are reasonably well recovered in the region of the megathrust

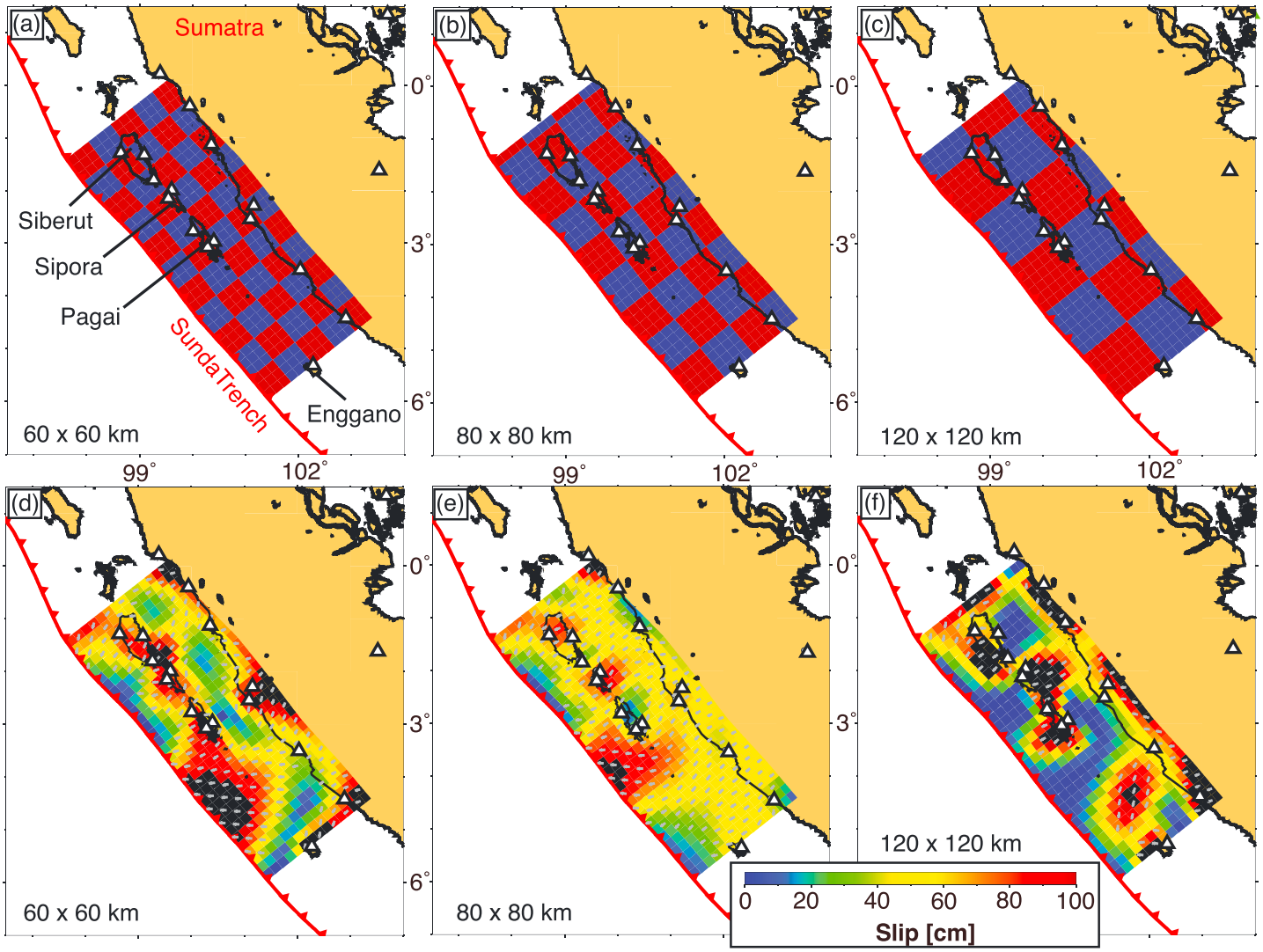


**Figure 7.** Checkerboard tests with various sizes of input checks: (a) 60 × 60 km, (b) 80 × 80 km, and (c) 120 × 120 km; and (d–f) recovery of slip in various parts of the fault model. The Laplacian smoothing weight is the same as that employed in our model results in Figure 4. White triangles: locations of the 17 SuGAr stations and 1 IGS station used in the inversion.

between Sipora and the Pagai Islands. Some slip checks are recovered at the Pagai Islands and along the Sumatran coast, downdip of the 2007 main shock rupture area, albeit with some smoothing of slip across neighboring fault patches. Our results suggest that afterslip under and west of the Pagai Islands is somewhat well resolved. In contrast, the checks are poorly recovered in regions close to the trench and over the majority of the region SE of the Pagai Islands (Figures 7d and 7e), which indicates that afterslip is poorly resolved in these regions. In order to resolve afterslip in these regions, we probe at where afterslip needs to occur on the fault by penalizing afterslip on different subfault patches and assessing the change in the data model fits (Figure S11 and Text S3).

We also performed forward models to determine how well the slip in key afterslip regions in our model are recovered. Synthetic slip of 1 m was assigned to patches located updip and downdip of the main shock rupture zone (Figures 8a and 8c), and we calculated displacements at each GPS station with the Okada model of elastic dislocations [*Okada*, 1985]. We applied the same Laplacian smoothing as that employed in our afterslip model that does not account for viscoelastic effects. Figures 8b and 8d indicate that although only ~50% of the slip magnitude is recovered, and that slip is smoothed across neighboring patches, the spatial distribution of slip is well estimated in both areas.

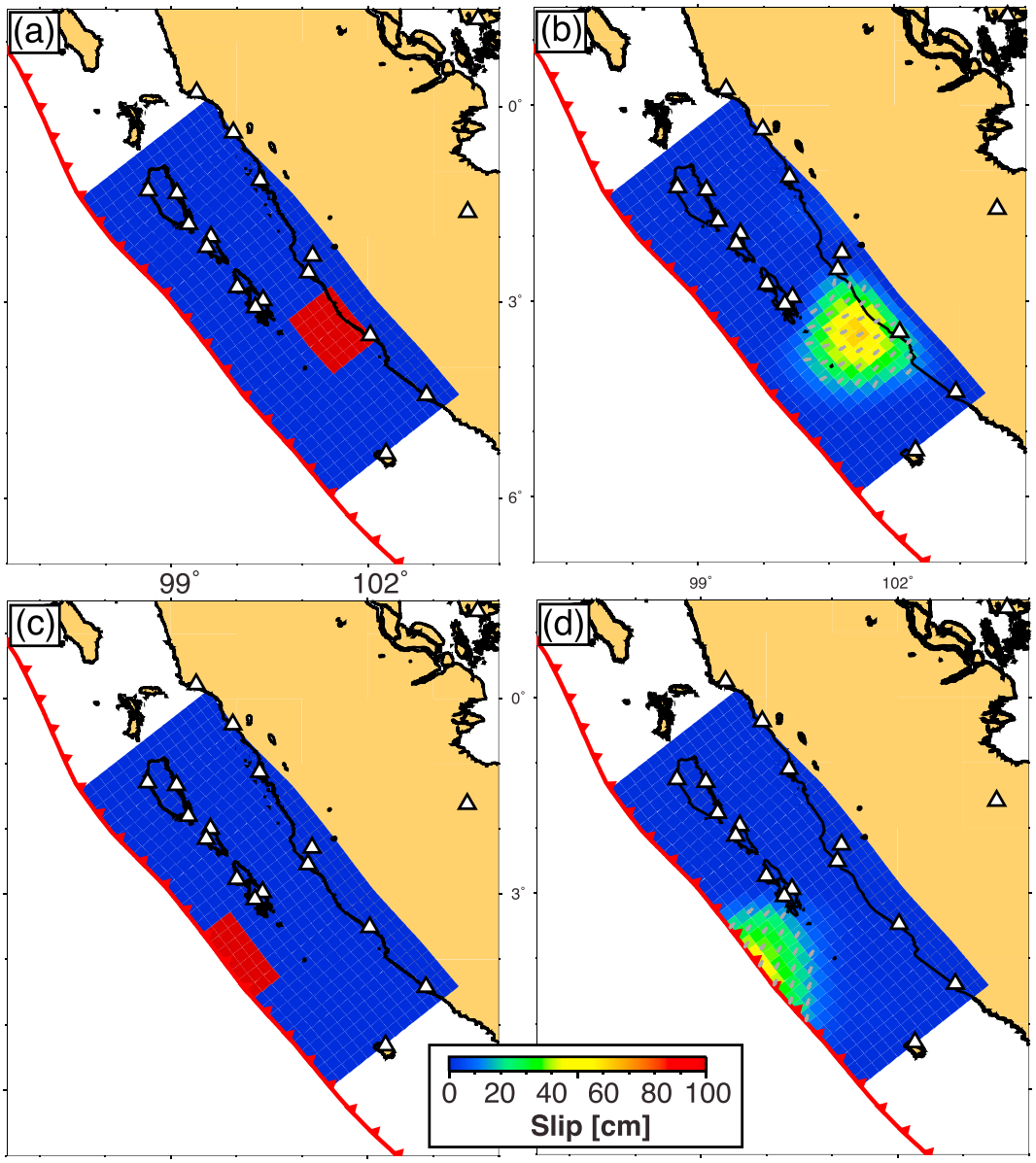


**Figure 8.** Recovery of synthetic slip patches in two key afterslip areas in the models: (a–b) downdip and (c–d) updip of the main shock rupture area. Figures 8a and 8c show the input synthetic slip distributions, and Figures 8b and 8d show the recovered slip distributions. We used the same Laplacian smoothing as that employed in our model in Figure 4. White triangles: Locations of GPS stations.

## 6. Discussion

Our model results suggest that reasonably well-resolved areas of afterslip are concentrated downdip of the 2007 coseismic rupture area and on a patch immediately west of the Pagai Islands. One of our main conclusions is that models accounting for viscoelastic effects yield significantly better data model fits than those that do not, suggesting that it is important to factor in deformation due to viscoelastic relaxation of the mantle. As expected, jointly inverting for strain in ductile shear zones and afterslip on the fault yields better data model fits than the traditional method of attempting to model and subtract the viscoelastic deformation from postseismic time series and inverting the residual time series (Figures S15–S17).

In the models that do not account for viscoelastic effects, a large amount of afterslip is concentrated downdip of the coseismic rupture zone, but which may actually represent viscoelastic deformation mapped onto the

megathrust. After incorporating ductile shear zones in a joint inversion of afterslip on the megathrust and strain in shear zones, less afterslip is concentrated downdip of the coseismic rupture area.

Afterslip in the downdip region occurs at depths ~30–75 km on the megathrust. Geodetic studies of fault coupling along the Sumatra subduction zone suggest that the downdip limit of the seismogenic zone in this region varies between 30 and 55 km, with predominantly creep at depths >55 km [*Chlieh et al.*, 2008; *Simoes et al.*, 2004], marking the depth of the seismic-aseismic downdip transition zone, where the onset of stable sliding and velocity-strengthening behavior may occur.

*Klein et al.* [2016] and *Trubienko et al.* [2014] propose that low-viscosity channels along the deepest part of the interface are required to explain the postseismic deformation patterns of the 2010 Maule earthquake, and 2004 Sumatra-Andaman earthquake, respectively. From the surface observations, it would be difficult to distinguish between the effects of low-viscosity channels from that of afterslip. It is beyond the scope of this study to model the combination of afterslip, relaxation within hypothesized low-viscosity channels as well as within the asthenosphere, since we do not have sufficient resolution for this event to model such complexities. However, for events where sufficient resolution is available, future work could implement our technique to model the effect of low-viscosity channels on the deformation field, via inverting for strains in shear zones that are designed to align along the megathrust interface.

In the shallow region of the megathrust, both models suggest a sizeable amount of cumulative afterslip updip of the 2007 main shock rupture area that borders and overlaps the 2010 Mentawai earthquake rupture area (region B in Figures 4a and 5a). We note that model resolution in the shallowest region of the fault is poor; this is shown by both checkerboard tests (Figure 7) and similar data model fits obtained in the case of penalizing afterslip on patches close to the trench (Figure S11).

The shallow afterslip in our models is located at similar depths to shallow afterslip observed after the 2005 Nias earthquake [*Hsu et al.*, 2006]. Our results are consistent with the general model described by *Marone et al.* [1991], in which coseismic rupture of the seismogenic zone causes stress perturbations in the updip zone of velocity-strengthening behavior, which are subsequently relaxed as afterslip. Researchers have commonly characterized subduction zone trench regions as aseismic, based primarily on two inferences: (1) that the updip limit of seismicity, defining a seismic front, is located at ~5–10 km depths on subduction zone megathrusts [*Byrne et al.*, 1988; *Lay and Bilek*, 2007; *Lay et al.*, 2012; *Tichelaar and Ruff*, 1993]; (2) that there is an abundance of materials at trench regions that exhibit velocity-strengthening behavior, such as unconsolidated sediments and smectite [*Byrne et al.*, 1988; *Moore and Saffer*, 2001; *Vrolijk*, 1990]. In addition, geodetic studies have regularly characterized the shallowest portions of megathrusts as aseismic, often as a result of unavailable model resolution in this region [*Chlieh et al.*, 2008]. However, it is clear that the seismic behavior of the shallow portion of the megathrust appears to be more complex than previously thought. Specifically, the shallow region of megathrusts can both participate in large earthquakes, as exemplified by the 2011 $M_w$ 9.0 Tohoku-oki earthquake, as well as host tsunami earthquakes, as exemplified by the 1314 and 2010 $M_w$ 7.8 Mentawai, 1992 $M_w$ 7.6 Nicaragua, 1994 $M_w$ 7.8 Java, and 1996 $M_w$ 7.5 Peru earthquakes [*Hill et al.*, 2012; *Philibosian et al.*, 2012; *Polet and Kanamori*, 2000]. The question that needs to be addressed is, therefore, what physical conditions and properties control the spatial and temporal pattern of shallow seismic ruptures?

A number of proposed models attempt to explain the spatial patterns of tsunami earthquake occurrence in the shallow portions of megathrusts. For example, *Polet and Kanamori* [2000] proposed that the subduction of rough, faulted oceanic plate increases the potential for a tsunami earthquake. *Lay and Bilek* [2007] highlighted the importance of considering temporally varying physical factors such as seafloor structures, pore fluid pressures, and strain rates. They proposed a model in which the region just downdip of the zone of stable sliding close to the trench consists of conditionally stable patches. These patches commonly slip aseismically but may occasionally fail coseismically in spatially distinct patches, if loaded at high strain rates [*Bilek and Lay*, 2002; *Bilek et al.*, 2004; *Lay et al.*, 2012; *Scholz*, 1998]. This model has been proposed based on far-field teleseismic data and inferred rigidities of materials in the shallow region of subduction zones, but support for this model requires examples that demonstrate the link between tsunami earthquake occurrence and a tectonic process capable of increasing strain rates in the shallow region. Possible processes that can cause high strain rates include afterslip and slow slip events. For example, along the weakly coupled section of the megathrust offshore Peru, a slow slip event and seismic sequence in 2009 preceded shallow rupture of the megathrust; the preceding events were proposed to promote eventual seismic rupture of conditionally stable patches in the shallow trench region [*Villegas-Lanza et al.*, 2016]. Coseismic weakening has also been proposed

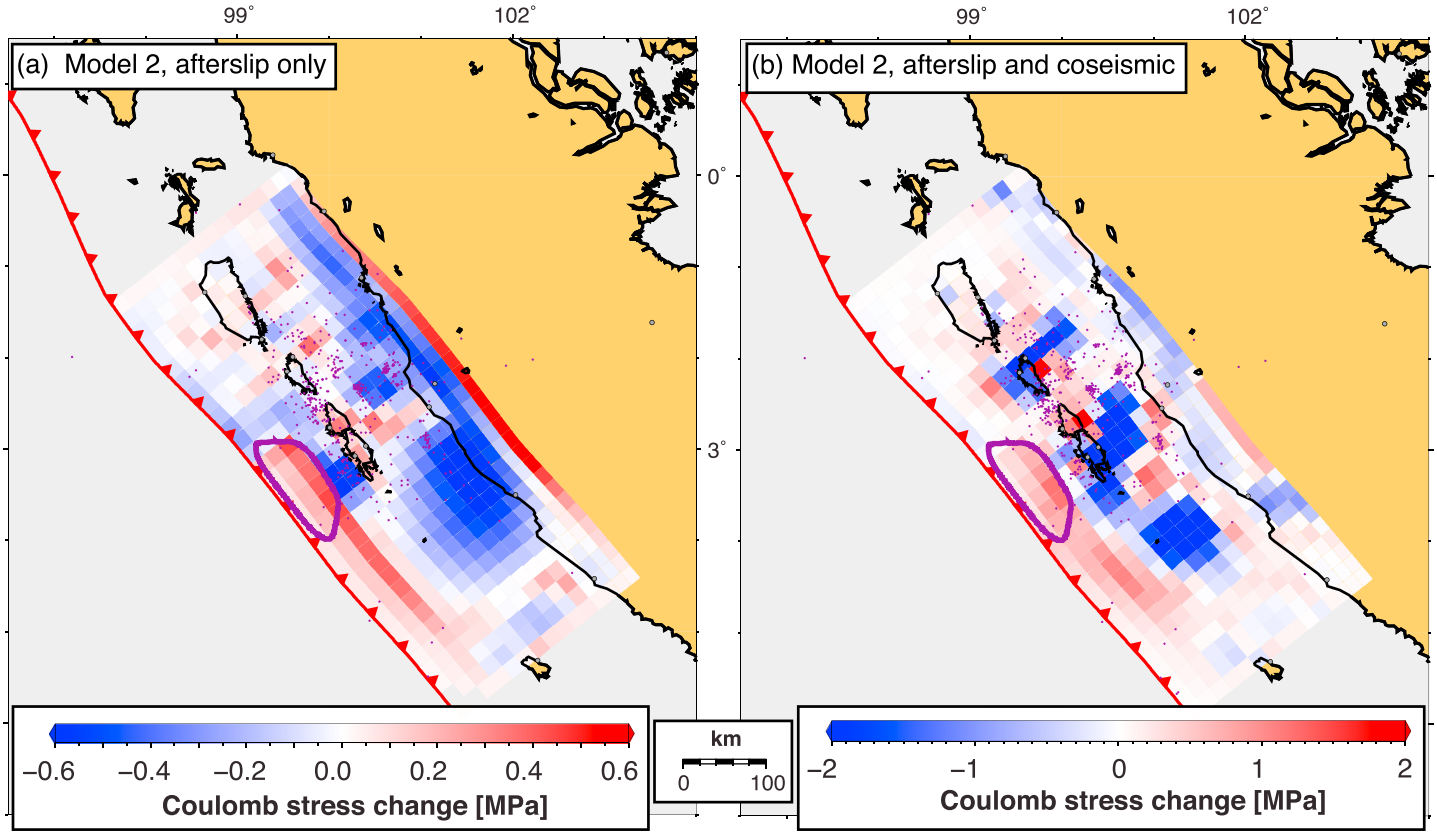


**Figure 9.** Coulomb stress changes from afterslip model that accounts for viscoelastic effects. Coulomb stress changes from (a) afterslip only, and (b) afterslip and coseismic slip collectively. A friction coefficient of 0.4 is assumed in the calculations. Purple contour: 1 m slip contour of the 2010 Mentawai earthquake [*Hill et al.*, 2012]. Purple circles: regional seismicity from *Collings et al.* [2012].

as a mechanism that facilitates large coseismic slip along shallow portions of megathrusts. Notably, in the 2011 Tohoku-oki earthquake, both the shallow and deeper parts of the megathrust ruptured in a single $M_w$ 9.0 event [*Bletery et al.*, 2014; *Ito et al.*, 2011; *Fujiwara et al.*, 2011]. Dynamic modeling studies suggest that producing Tohoku-oki scale earthquakes with recurrence times comparable to those found in the historical record requires coseismic weakening via efficient thermal pressurization in the shallow part of the megathrust, together with sufficiently rate-strengthening behavior [*Cubas et al.*, 2015]. It would be relevant for future studies to investigate the mechanisms and frictional properties that would favor ruptures of the deeper and shallower parts of the megathrust in two isolated events, with the length of time delay between events similar to that between the 2007 and 2010 ruptures in Sumatra. In addition, *Kuncoro et al.* [2015] proposed that low effective friction along the shallow part of the megathrust is required to cause eventual coseismic rupture of the trench region and that this low effective friction could be achieved via coseismic weakening. We speculate that afterslip may enhance the coseismic weakening of the trench region that leads to successive buildup of high pore pressures and hence low effective friction, facilitating eventual coseismic rupture of the trench region.

We hypothesize that shallow afterslip regions in our models caused localized increases in strain rates and stresses adjacent to and within the Mentawai earthquake rupture area. These stresses, probably in concert with coseismic stresses, promoted rupture of the trench region in 2010. In order to test this hypothesis, we calculated Coulomb stress changes based on our model that penalizes afterslip on shallow patches in and southeast of the Mentawai earthquake rupture area (Figure S11; details of our method are described in Text S5). In this way, we adopt the conservative stance of only estimating Coulomb stress changes from afterslip on well-resolved patches. Figure 9a suggests that afterslip caused ~0.1–0.4 MPa of positive Coulomb stress change updip of the 2007 main shock rupture area. In addition, Figure 9b shows that both afterslip and coseismic slip caused a maximum positive Coulomb stress change of ~1.2 MPa in the Mentawai earthquake rupture area, which is higher than elsewhere along strike in the trench region, potentially rendering this area

more likely to rupture coseismically compared to other regions along strike. These results suggest that localized increases in strain rates and Coulomb stress changes due to shallow afterslip may have brought forward in time coseismic failure of the trench region in 2010. Putting our findings in the context of *Lay and Bilek*'s [2007] model, the 2010 Mentawai earthquake may represent coseismic rupture of a spatially distinct patch of conditional stability on the fault. The fact that the region closest to the trench ruptured in this earthquake implies that these conditionally stable patches can exist all the way to the trench.

*Feng et al.* [2016] modeled the afterslip following the Mentawai earthquake and found that in order to explain the postseismic deformation following the earthquake, their models need to include an ~0.1 MPa difference in pre-earthquake Coulomb stress between the northwestern and southeastern portions of the afterslip area. This stress difference likely reflects the spatial distribution of stress changes caused by the 2007 coseismic and postseismic sequence. We calculated the difference in Coulomb stress change between the northwestern and southeastern portions defined by the ~50 cm afterslip area for their model and found a similar ~0.1–0.2 MPa difference in stress change between the two portions. This similar result implies that the stress changes from our model are consistent with the prestress required in this region in order to explain the afterslip following the Mentawai earthquake.

Some researchers have highlighted the importance of considering the role of décollements and structures in the accretionary wedge that facilitate coseismic rupture of the shallow regions of subduction zones [e.g., *Hubbard et al.*, 2015]. Bathymetric maps and seismic reflection results in the 2010 Mentawai earthquake rupture area reveal paired thrust faults associated with fold and thrust belts at the toe of the accretionary wedge that likely slipped coseismically during the 2010 event and played an important role in tsunamigenesis [*Singh et al.*, 2011]. Geodetic models of coseismic slip and afterslip should ideally take into account these mapped structures in trench regions. Such efforts are currently limited by the lack of model resolution in trench regions, but with the advent of seafloor geodetic networks installed at an increasing number of subduction zones worldwide, geodesists may begin to explore these models.

The geodetic moment of our coseismic slip distribution model is $4.18 \times 10^{21}$ N m, which is similar to a value of $5 \times 10^{21}$ N m obtained by *Konca et al.* [2008]. Our afterslip models suggest cumulative afterslip geodetic moments ranging from 3.55 to $4.02 \times 10^{21}$ N m, equivalent to a moment magnitude of $M_w$ 8.3–8.4, and which amounts to ~85 to 95% of the coseismic geodetic moment. The 2007 coseismic and afterslip geodetic moment amounts to $\sim 7.73–8.20 \times 10^{21}$ N m. The geodetic moment of the 2007 and 2010 sequences collectively represents ~30–44% of the moment estimated to have been released during the 1833 earthquake ($M_w$ 8.8–8.9 [*Philibosian et al.*, 2014]). We caution though, that this is only a first-order estimate, since there are uncertainties in the amount of seismic moment released along this section of the megathrust during the 1833 earthquake, and we have evidence that elsewhere in Sumatra (and therefore perhaps here too) rates of interseismic strain accumulation may not be constant over time [*Meltzner et al.*, 2015; *Tsang et al.*, 2015].

## 7. Conclusions

To understand the behavior of the southern Mentawai section of the megathrust during the modern sequence of events, we have modeled the coseismic slip and ensuing afterslip of the 2007 Bengkulu earthquake, using improved coseismic offsets and long-term postseismic time series, respectively. Our results suggest that accounting for viscoelastic deformation in the inversion reduces the magnitude of afterslip in the region downdip of the 2007 main shock rupture area. Our results suggest that afterslip occurs within, updip, and downdip of the 2007 main shock rupture area. One of our most important results is that the shallow patches of afterslip border and overlap the 2010 Mentawai earthquake rupture zone. We propose that the localized increases in strain rates and stresses caused by the coseismic slip and ensuing shallow afterslip may have brought forward in time coseismic failure of the shallow portion of the megathrust in 2010.

**Acknowledgments**
The SuGAr daily RINEX files are available for public download at ftp://eos.ntu.edu.sg/SugarData, with a latency of 3 months. This research was supported by the National Research Foundation Singapore under its Singapore NRF Fellowship scheme (NRF awards NRF-NRFF2010-064 and NRF-NRFF2013-04), by the Earth Observatory of Singapore (EOS), by the Singapore Ministry of Education (MOE) under the Research Centers of Excellence initiative, and by a Nanyang Technological University Startup grant. L.Tsang was supported by a Singapore International Graduate Award and an EOS research scholarship. We are grateful for linguistic advice from P. Adamek. We thank K. Sieh, J. Freymueller, A. Lubis, B. Philibosian, R. Salman, B. Meade, and T. Dixon for insightful discussions. We express our thanks to the Editor Y. Ben-Zion, Associate Editor Laura Wallace, and two reviewers for their detailed and helpful comments and suggestions that have improved the paper. This work comprises Earth Observatory of Singapore contribution 126.

## References

Altamimi, Z., L. Mtivier, and X. Collilieux (2012), ITRF2008 plate motion model, *J. Geophys. Res. Solid Earth*, *117*, B07402, doi:10.1029/2011JB008930.

Barbot, S., and Y. Fialko (2010a), A unified continuum representation of post-seismic relaxation mechanisms: semi-analytic models of afterslip, poroelastic rebound and viscoelastic flow, *Geophys. J. Int.*, *182*(3), 1124–1140, doi:10.1111/j.1365-246X.2010.04678.x.

Barbot, S., and Y. Fialko (2010b), Fourier-domain Green's function for an elastic semi-infinite solid under gravity, with applications to earthquake and volcano deformation, *Geophys. J. Int.*, *182*(2), 568–582, doi:10.1111/j.1365-246X.2010.04655.x.

Barbot, S., Y. Fialko, and Y. Bock (2009), Postseismic deformation due to the $M_w$ 6.0 2004 Parkfield earthquake: Stress-driven creep on a fault with spatially variable rate-and-state friction parameters, *J. Geophys. Res. Solid Earth*, *114*, B07405, doi:10.1029/2008JB005748.

Bilek, S. L., and T. Lay (2002), Tsunami earthquakes possibly widespread manifestations of frictional conditional stability, *Geophys. Res. Lett.*, *29*(14), 1673, doi:10.1029/2002GL015215.

Bilek, S. L., T. Lay, and L. J. Ruff (2004), Radiated seismic energy and earthquake source duration variations from teleseismic source time functions for shallow subduction zone thrust earthquakes, *J. Geophys. Res. Solid Earth*, *109*, B09308, doi:10.1029/2004JB003039.

Bletery, Q, A. Sladen, B. Delouis, M. Vallée, J.-M. Nocquet, L. Rolland, and J. Jiang (2014), A detailed source model for the $M_w$ 9. 0 Tohoku-Oki earthquake reconciling geodesy, seismology, and tsunami records, *J. Geophys. Res. Solid Earth*, *119*, 7636–7653, doi:10.1002/2014JB011261.

Bruhat, L., S. Barbot, and J.-P. Avouac (2011), Evidence for postseismic deformation of the lower crust following the 2004 $M_w$ 6.0 Parkfield earthquake, *J. Geophys. Res. Solid Earth*, *116*, B08401, doi:10.1029/2010JB008073.

Byrne, D. E., D. M. Davis, and L. R. Sykes (1988), Loci and maximum size of thrust earthquakes and the mechanics of the shallow region of subduction zones, *Tectonics*, *7*(4), 833–857, doi:10.1029/TC007i004p00833.

Chlieh, J. P. A., K. Sieh, D. H. Natawidjaja, and J. Galetzka (2008), Heterogeneous coupling of the Sumatran megathrust constrained by geodetic and paleogeodetic measurements, *J. Geophys. Res. Solid Earth*, *113*, B05305, doi:10.1029/2007JB004981.

Collings, R., D. Lange, A. Rietbrock, F. Tilmann, D. Natawidjaja, B. Suwargadi, M. Miller, and J. Saul (2012), Structure and seismogenic properties of the Mentawai segment of the Sumatra subduction zone revealed by local earthquake traveltime tomography, *J. Geophys. Res.*, *117*, B01312, doi:10.1029/2011JB008469.

Cubas, N., N. Lapusta, J.-P. Avouac, and H. Perfettini (2015), Numerical modeling of long-term earthquake sequences on the NE Japan megathrust: Comparison with observations and implications for fault friction, *Earth Planet. Sci. Lett.*, *419*, 187–198, doi:10.1016/j.epsl.2015.03.002.

Feng, L., E. M. Hill, P. Banerjee, I. Hermawan, L. L. H. Tsang, D. H. Natawidjaja, B. W. Suwargadi, and K. Sieh (2015), A unified GPS-based earthquake catalog for the Sumatran plate boundary between 2002 and 2013, *J. Geophys. Res. Solid Earth*, *120*, 3566–3598, doi:10.1002/2015JB012503.

Feng, L., S. Barbot, E. M. Hill, I. Hermawan, P. Banerjee, and D. H. Natawidjaja (2016), Footprints of past earthquakes revealed in the afterslip of the 2010 $M_w$ 7.8 Mentawai tsunami earthquake, *Geophys. Res. Lett.*, *43*(18), 9518–9526, doi:10.1002/2016GL069870.

Fujiwara, T., S. Kodaira, T. No, Y. Kaiho, N. Takahashi, and Y. Kaneda (2011), The 2011 Tohoku-Oki earthquake: Displacement reaching the trench axis, *Science*, *334*(6060), 1240, doi:10.1126/science.1211554.

Hayes, G. P., D. J. Wald, and R. L. Johnson (2012), Slab1.0: A three-dimensional model of global subduction zone geometries, *J. Geophys. Res. Solid Earth*, *117*, B01302, doi:10.1029/2011JB008524.

Hill, E. M., et al. (2012), The 2010 $M_w$ 7.8 Mentawai earthquake: Very shallow source of a rare tsunami earthquake determined from tsunami field survey and near-field GPS data, *J. Geophys. Res. Solid Earth*, *117*, B06402, doi:10.1029/2012JB009159.

Hsu, Y.-J., M. Simons, J.-P. Avouac, J. Galetzka, K. Sieh, M. Chlieh, D. Natawidjaja, L. Prawirodirdjo, and Y. Bock (2006), Frictional afterslip following the 2005 Nias-Simeulue earthquake, Sumatra, *Science*, *312*(5782), 1921–1926, doi:10.1126/science.1126960.

Hubbard, J., S. Barbot, E. M. Hill, and P. Tapponnier (2015), Coseismic slip on shallow décollement megathrusts: Implications for seismic and tsunami hazard, *Earth Sci. Rev.*, *141*, 45–55, doi:10.1016/j.earscirev.2014.11.003.

Ito, Y., T. Tsuji, Y. Osada, M. Kido, D. Inazu, Y. Hayashi, H. Tsushima, Hino R., and H. Fujimoto (2011), Frontal wedge deformation near the source region of the 2011 Tohoku-Oki earthquake, *Geophys. Res. Lett.*, *38*, L00G05, doi:10.1029/2011GL048355.

Karato, S.-I. (2010), Rheology of the deep upper mantle and its implications for the preservation of the continental roots: A review, *Tectonophysics*, *481*(14), 82–98, doi:10.1016/j.tecto.2009.04.011.

Klein, E., L. Fleitout, C. Vigny, and J. D. Garaud (2016), Afterslip and viscoelastic relaxation model inferred from the large-scale post-seismic deformation following the 2010 $M_w$ 8.8 Maule earthquake (Chile), *Geophys. J. Int.*, *205*(3), 1455–1472, doi:10.1093/gji/ggw086.

Konca, A. O., et al. (2008), Partial rupture of a locked patch of the Sumatra megathrust during the 2007 earthquake sequence, *Nature*, *456*(7222), 631–635, doi:10.1038/nature07572.

Kositsky, A. P., and J. P. Avouac (2010), Inverting geodetic time series with a principal component analysis-based inversion method, *J. Geophys. Res. Solid Earth*, *115*, B03401, doi:10.1029/2009JB006535.

Kumar, P., X. Yuan, M. R. Kumar, R. Kind, X. Li, and R. K. Chadha (2007), The rapid drift of the Indian tectonic plate, *Nature*, *449*(7164), 894–897, doi:10.1038/nature06214.

Kuncoro, A., N. Cubas, S. C. Singh, M. Etchebes, and P. Tapponnier (2015), Tsunamigenic potential due to frontal rupturing in the Sumatra locked zone, *Earth Planet. Sci. Lett.*, *432*, 311–322, doi:10.1016/j.epsl.2015.10.007.

Lay, T., and S. Bilek (2007), Anomalous earthquake ruptures at shallow depths on subduction zone megathrusts, in *The seismogenic zone of subduction thrust faults*, vol. 1, edited by T. Lay and S. Bilek, pp. 476–511, Columbia Univ. Press, New York.

Lay, T., H. Kanamori, C. J. Ammon, K. D. Koper, A. R. Hutko, L. Ye, H. Yue, and T. M. Rushing (2012), Depth-varying rupture properties of subduction zone megathrust faults, *J. Geophys. Res.*, *117*, B04311, doi:10.1029/2011JB009133.

Lubis, A. M., A. Hashima, and T. Sato (2012), Analysis of afterslip distribution following the 2007 September 12 southern Sumatra earthquake using poroelastic and viscoelastic media, *Geophys. J. Int.*, *192*(1), 18–37, doi:10.1093/gji/ggs020.

Marone, C. J., C. H. Scholtz, and R. Bilham (1991), On the mechanics of earthquake afterslip, *J. Geophys. Res. Solid Earth*, *96*, 8441–8452, doi:10.1029/91JB00275.

Meade, B. J., Y. Klinger, and E. A. Hetland (2013), Inference of multiple earthquake cycle relaxation timescales from irregular geodetic sampling of interseismic deformation, *Bull. Seismol. Soc. Am.*, *103*(5), 2824–2835, doi:10.1785/0120130006.

Meltzner, A. J., et al. (2015), Time-varying interseismic strain rates and similar seismic ruptures on the Nias-Simeulue patch of the Sunda megathrust, *Quarternary Sci. Rev.*, *122*, 258–281, doi:10.1016/j.quascirev.2015.06.003.

Miyazaki, S., P. Segall, J. Fukuda, and T. Kato (2004), Space time distribution of afterslip following the 2003 Tokachi-Oki earthquake: Implications for variations in fault zone frictional properties, *Geophys. Res. Lett.*, *31*, L06623, doi:10.1029/2003GL019410.

Moore, J. C., and D. Saffer (2001), Updip limit of the seismogenic zone beneath the accretionary prism of southwest Japan: An effect of diagenetic to low-grade metamorphic processes and increasing effective stress, *Geology*, *29*(2), 183–186, doi:10.1130/0091-7613(2001)029<0183:ulotsz>2.0.co;2.

Okada, Y. (1985), Surface deformation due to shear and tensile faults in a half-space, *Bull. Seismol. Soc. Am.*, *75*(4), 1135–1154.

Panet, I., V. Mikhailov, M. Diament, F. Pollitz, G. King, O. De Viron, M. Holschneider, R. Biancale, and J.-M. Lemoine (2007), Coseismic and post-seismic signatures of the Sumatra 2004 December and 2005 March earthquakes in GRACE satellite gravity, *Geophys. J. Int.*, *171*(1), 177–190, doi:10.1111/j.1365-246X.2007.03525.x.

Philibosian, B., K. Sieh, D. H. Natawidjaja, H.-W. Chiang, C.-C. Shen, B. W. Suwargadi, E. M. Hill, and R. L. Edwards (2012), An ancient shallow slip event on the Mentawai segment of the Sunda megathrust, Sumatra, *J. Geophys. Res. Solid Earth*, *117*, B05401, doi:10.1029/2011JB009075.

Philibosian, B., K. Sieh, J.-P. Avouac, D. H. Natawidjaja, H.-W. Chiang, C.-C. Wu, H. Perfettini, C.-C. Shen, M. R. Daryono, and B. W. Suwargadi (2014), Rupture and variable coupling behavior of the Mentawai segment of the Sunda megathrust during the supercycle culmination of 1797 to 1833, *J. Geophys. Res. Solid Earth*, *119*, 7258–7287, doi:10.1002/2014JB011200.

Polet, J., and H. Kanamori (2000), Shallow subduction zone earthquakes and their tsunamigenic potential, *Geophys. J. Int.*, *142*(3), 684–702, doi:10.1046/j.1365-246x.2000.00205.x.

Pollitz, R. B., and P. Banerjee (2006), Post-seismic relaxation following the great 2004 Sumatra-Andaman earthquake on a compressible self-gravitating Earth, *Geophys. J. Int.*, *167*(1), 397–420, doi:10.1111/j.1365-246X.2006.03018.x.

Rollins, C., S. Barbot, and J.-P. Avouac (2015), Postseismic deformation following the 2010 $M = 7.2$ El Mayor-Cucapah earthquake: Observations, kinematic inversions, and dynamic models, *Pure Appl. Geophys.*, *172*(5), 1305–1358, doi:10.1007/s00024-014-1005-6.

Rousset, B., S. Barbot, J.-P. Avouac, and Y.-J. Hsu (2012), Postseismic deformation following the 1999 Chi-Chi earthquake, Taiwan: Implication for lower-crust rheology, *J. Geophys. Res.*, *117*, B12405, doi:10.1029/2012JB009571.

Scholz, C. H. (1998), Earthquakes and friction laws, *Nature*, *391*(6662), 37–42, doi:10.1038/34097.

Shearer, P., and R. Bürgmann (2010), Lessons learned from the 2004 Sumatra-Andaman megathrust rupture, *Annu. Rev. Earth Planet. Sci.*, *38*(1), 103–131, doi:10.1146/annurev-earth-040809-152537.

Sieh, K. (2007), The Sunda megathrust — Past, present and future, *J. Earthquake Tsunami*, *01*(01), 1–19, doi:10.1142/S179343110700002X.

Sieh, K., D. H. Natawidjaja, A. J. Meltzner, C.-C. Shen, H. Cheng, K.-S. Li, B. W. Suwargadi, J. Galetzka, B. Philibosian, and R. L. Edwards (2008), Earthquake supercycles inferred from sea-level changes recorded in the corals of west Sumatra, *Science*, *322*(5908), 1674–1678, doi:10.1126/science.1163589.

Simoes, M., J. P. Avouac, R. Cattin, and P. Henry (2004), The Sumatra subduction zone: A case for a locked fault zone extending into the mantle, *J. Geophys. Res. Solid Earth*, *109*, B10402, doi:10.1029/2003JB002958.

Singh, S. C., N. Hananto, M. Mukti, H. Permana, Y. Djajadihardja, and H. Harjono (2011), Seismic images of the megathrust rupture during the 25th October 2010 Pagai earthquake, SW Sumatra: Frontal rupture and large tsunami, *Geophys. Res. Lett.*, *38*, L16313, doi:10.1029/2011GL048935.

Suito, H., and J. T. Freymueller (2009), A viscoelastic and afterslip postseismic deformation model for the 1964 Alaska earthquake, *J. Geophys. Res. Solid Earth*, *114*, B11404, doi:10.1029/2008JB005954.

Tichelaar, B. W., and L. J. Ruff (1993), Depth of seismic coupling along subduction zones, *J. Geophys. Res. Solid Earth*, *98*(B2), 2017–2037, doi:10.1029/92JB02045.

Trubienko, O., J.-D. Garaud, and L. Fleitout (2014), Models of postseismic deformation after megaearthquakes: The role of various rheological and geometrical parameters of the subduction zone, *Solid Earth Discuss.*, *6*(1), 427–466, doi:10.5194/sed-6-427-2014.

Tsang, L. L. H., A. J. Meltzner, E. M. Hill, J. T. Freymueller, and K. Sieh (2015), A paleogeodetic record of variable interseismic rates and megathrust coupling at Simeulue Island, Sumatra, *Geophys. Res. Lett.*, *42*, 10585–10594, doi:10.1002/2015GL066366.

Villegas-Lanza, J.-M. N., F. Rolandone, M. Valle, H. Tavera, F. Bondoux, T. Tran, X. Martin, and M. Chlieh (2016), A mixed seismic-aseismic stress release episode in the Andean subduction zone, *Nature Geosci.*, *9*, 150–154, doi:10.1038/NGEO2620.

Vrolijk, P. (1990), On the mechanical role of smectite in subduction zones, *Geology*, *18*(8), 703–707, doi:10.1130/0091-7613(1990)018<0703:otmros>2.3.co;2.

Yue, H., T. Lay, L. Rivera, Y. Bai, Y. Yamazaki, K. F. Cheung, E. M. Hill, K. Sieh, W. Kongko, and A. Muhari (2014), Rupture process of the 2010 $M_W$ 7.8 Mentawai tsunami earthquake from joint inversion of near-field hr-GPS and teleseismic body wave recordings constrained by tsunami observations, *J. Geophys. Res. Solid Earth*, *119*, 5574–5593, doi:10.1002/2014JB011082.

Zumberge, J. F., M. B. Heflin, D. C. Jefferson, M. M. Watkins, and F. H. Webb (1997), Precise point positioning for the efficient and robust analysis of GPS data from large networks, *J. Geophys. Res. Solid Earth*, *102*(B3), 5005–5017, doi:10.1029/96JB03860.